Theoretical Studies of Dissociative Recombination
S.L. Guberman

Reprinted from **Thermophysical Aspects of Re-entry Flows**, edited by James N. Moss and Carl D. Scott, Vol. 103 of Progress in Astronautics and Aeronautics series. Published in 1986 by the American Institute of Aeronautics and Astronautics, Inc., 1633 Broadway, N.Y. 10019, 626 pp., 6×9, illus., ISBN 0-930403-10-X, $59.50 Member, $79.50 List.

Theoretical Studies of Dissociative Recombination

Steven L. Guberman*
Institute for Scientific Research, Stoneham, Massachusetts
and
Harvard-Smithsonian Center for Astrophysics, Cambridge, Massachusetts

Abstract

The calculation of dissociative recombination rates and cross sections over a wide temperature range by theoretical quantum chemical techniques is described. Model calculations on electron capture by diatomic ions are reported that illustrate the dependence of the rates and cross sections on electron energy, electron temperature, and vibrational temperature for three model crossings of neutral and ionic potential curves. Using harmonic oscillator vibrational wave functions, it is shown that cross sections for recombination to the lowest vibrational level of the ion can vary by several orders of magnitude, depending upon the position of the neutral and ionic potential curve crossing within the turning points of the v=1 vibrational level. A new approach for calculating electron capture widths is reported. Ab initio calculations are described for recombination of O_2^+ leading to excited O atoms.

I. Introduction

Models[1,2] of the shock layer encountered by an aeroassisted orbital transfer vehicle (AOTV) require as input accurate cross sections and rate constants for the atomic and molecular processes that characterize the shock radiation. From the estimated atomic and molecular densities[2] in the shock layer and the expected residence time of 1ms[1], it can be expected that electron-ion collision processes will be important in the shock model. Dissociative recombination (DR) of molecular ions with electrons,

---

Presented as Paper 85-1037 at the AIAA 20th Thermophysics Conference, Williamsburg, VA, June 19-21, 1985.

* Physicist.

e.g. $O_2^+ + e^- \rightarrow O + O$, can be expected to be of major importance since these processes are known to have high rates (e.g. $10^{-7}cm^3/s$) at room temperature. However, there have been no experimental measurements of DR at the high temperatures that are expected to characterize the shock layer. Indeed, even at room temperature, it is difficult to perform experiments that determine the dependence of the translational energy and quantum yields of the product atoms on the electronic and vibrational states of the reactant molecular ions. Section II contains a discussion of the DR mechanism. Several model calculations are reported in Sec. III that demonstrate the dependence of DR rates and cross sections upon the position of the crossing between the neutral and ion potential energy curves. The need for accurately determined potential curves is demonstrated. The ab initio calculation of potential curves and electronic widths is described in Secs. IV and V respectively. An application of ab initio theoretical techniques to one channel in the DR of O_2^+ is presented in Sec. VI.

II. Mechanism

The mechanism of DR was first described by Bates[3] and later by Bardsley[4] and is illustrated in Fig. 1. For a diatomic ion in the v=0 vibrational level and for capture only into the neutral state labeled A, an electron with energy ε (shown by the vertical line) will have a high probability for capture at the internuclear distance (R) corresponding to the vertical line if the vibrational wave functions for the ion and neutral states have a high overlap at this point. After the electron is captured into the repulsive state, the nuclei begin to fly apart. While flying apart, the molecule can emit the electron leaving an ion in the v=0,1, or 2 vibrational levels for the initial electron energy shown in Fig.1. If the ion is left in v=1 or 2, the net result is vibrational excitation with the neutral repulsive state acting as an intermediate resonance. However, if the nuclei should separate on the neutral potential curve to an internuclear distance greater than the distance of the crossing between the ion and neutral curves, autoionization becomes unlikely.

Whether autoionization or dissociation is favored depends upon a number of factors discussed below, including the relative positions of the ion and neutral potential curves, the magnitude of the electron capture widths, the electron energy, and the extent of vibrational excitation. The role of some of these factors is discussed in the model examples given in the next section. Dissociation times are

usually fast compared to autoionization lifetimes, so that electron/molecular ion recombination at low electron temperatures can proceed at rates that can often be five orders of magnitude faster than electron-atomic ion recombination. This mechanism is referred to as direct recombination.[4]

The indirect recombination mechanism[5] involves initial capture of the electron by the molecular ion into an excited vibrational level of a bound Rydberg state. The Rydberg state is then predissociated by the same repulsive states responsible for direct recombination. While indirect recombination causes detailed structure to enter into the electron energy dependence of the recombination cross section,[6,7] it generally does not alter the overall shape of the cross section. In this paper we will restrict the discussion to direct recombination.

III. Model Calculations

The expression for the cross section σ for direct DR from vibrational level v has been derived from resonant scattering theory[6] and quantum defect theory.[7] The quantum defect theory expression is given by

$$\sigma_v=(\pi r/2k_e^2)[4\xi_v/(1+\sum_{v'}\xi_{v'})^2] \qquad (1)$$

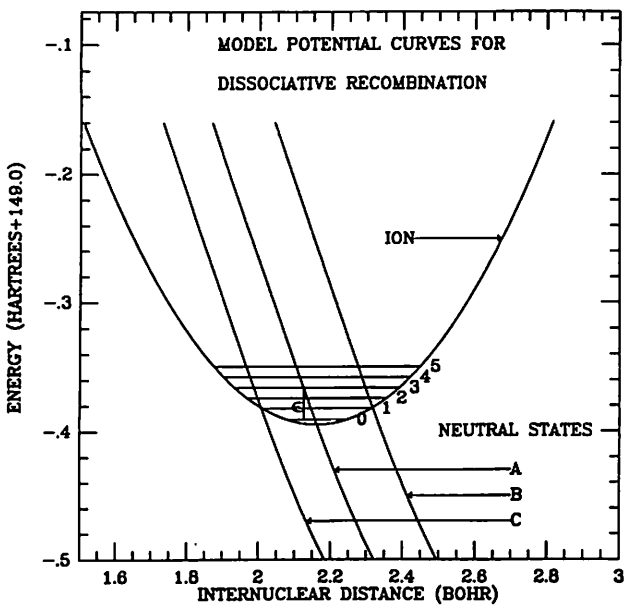

Fig. 1 Potential curves for three model crossings of neutral dissociative states with a bound ion.

where k_e is the wave number of the incident electron and r the ratio of multiplicities of the neutral and ion states. The matrix elements ξ_v are given by

$$\xi_v=(\pi/2)[\langle X_v|\Gamma^{1/2}(R)|X_d\rangle]^2 \qquad (2)$$

where X_v and X_d are vibrational wave functions for the ion and dissociative states, respectively. $\Gamma(R)$ is the width that connects the electronic continuum of the free electron and ion to the repulsive dissociating resonance state. The integration is over both R and the electronic coordinates. The electronic Hamiltonian H couples these two electronic states with

$$\Gamma(R)=2\pi\langle\{\Phi_{ion}(x,R)\phi_\varepsilon(x,R)\}|H|\Phi_d(x,R)\rangle^2 \qquad (3)$$

where the integration is over the electronic coordinates represented by x and the wave functions from left to right in Eq.(3) are for the ion core, the free electron, and the dissociative neutral state. The {} denote the antisymmetrized product of the ion core and free electron wave functions.

In order to calculate from first principles the cross section for DR, one needs wave functions for the ion and neutral states, potentials in which the nuclear wave functions can be calculated, and the matrix elements shown in Eqs.(2) and (3). Before reviewing the ab initio calculation of these quantities, it is instructive to examine the electron energy dependence of the cross sections and rate constants for DR upon the variation of the crossing point of the neutral and ionic curves. The three model crossings to be examined are shown in Fig. 1. For the cross section and rate constant calculations, a representative width of 0.30 eV, which is constant with internuclear distance(R), has been chosen. The use of a constant width is a good approximation for cases such as O_2 where the diabatic repulsive states do not change character with R near the ion potential curve. Each of the neutral curves in Fig. 1 has the same slope of about 20eV per atomic unit near the ion. In Eq. (1), we take r=1.5 corresponding, for example, to the capture of an electron into a $^3\Pi$ neutral state by an ion in a $^2\Pi$ state. In the calculations, we take the ion curve in Fig. 1 to be that for a harmonic oscillator and include the lowest six vibrational levels. A fundamental frequency of 1905.13 cm^{-1} appropriate for the ground state of O_2^+ was used.[8] Since the width is taken to be constant with variation of the internuclear distance, the matrix element in Eq. (2) can be factored into a product of Γ and a

Franck-Condon factor. The Franck-Condon factor is particularly large from v=0 for neutral curve A at low electron energies. The large Franck-Condon factor leads to both a high capture probability and also to a high probability that the electron will be ejected after capture.

The role of autoionization in reducing the DR cross section is given by the second denominator in Eq. (1). Figure 2 shows the cross section for dissociative recombination through v=0 of neutral curve A for both including [Eq. (1)] and excluding autoionization. In the latter case, the second denominator in Eq. (1) is set to unity. At low electron energies the cross section for DR is reduced by a factor of 0.8 by autoionization. Also the cross section closely follows an inverse electron energy dependence $(1/k_e^2)$, indicating that at low energies, for the case A curve crossing, the Franck-Condon factor varies only slowly with electron energy. At higher electron energies, the cross section falls off more rapidly due to the rapid decrease of the vibrational overlap. Indeed, between 2 and 5 eV, the cross section decreases by three orders of magnitude. A break occurs in the cross section just above 0.24 eV and is due to the opening of a new autoionization channel in which the ion is left in the v=1

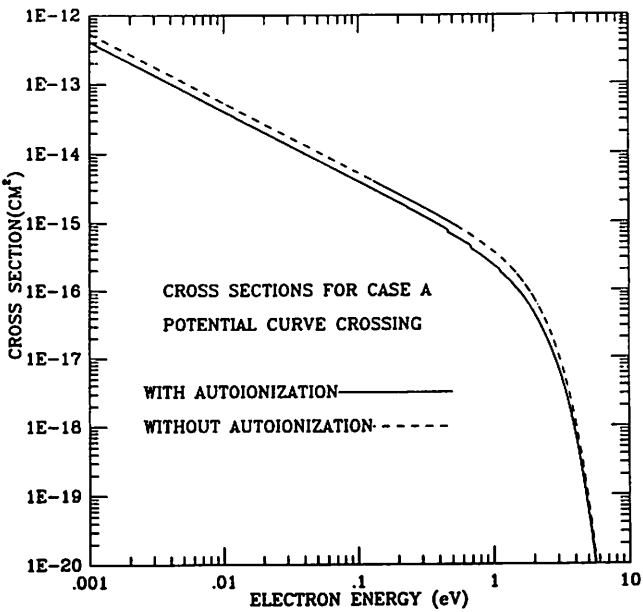

Fig. 2 DR from v=0 for a neutral curve crossing near the minimum of the ion potential curve.

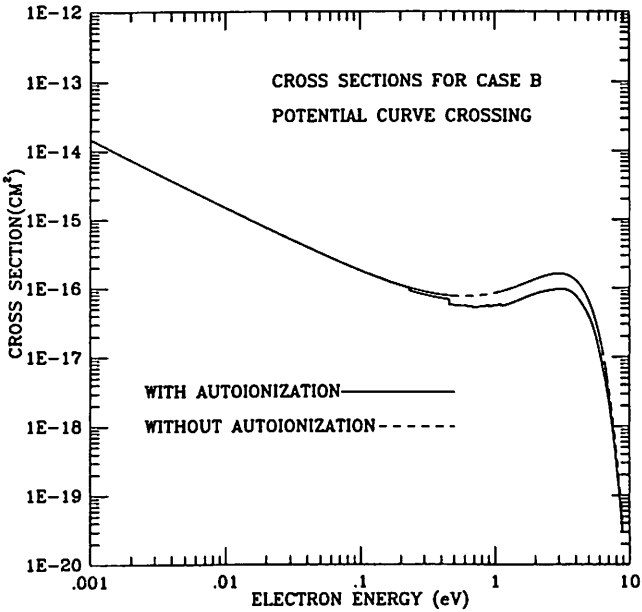

Fig. 3 DR from v=0 for a neutral curve crossing near the large R turning point of the v=1 level of the ion.

vibrational level. Breaks at higher energies correspond to the opening of autoionization channels through higher ion vibrational levels. The break near 0.45 eV for v=2 is larger than the v=1 break because, at these electron energies for neutral curve A, the continuum vibrational wave function is near a node in the v=1 wave function, but near a maximum in the v=2 wave function. Converging to each ion vibrational level from below is an infinite number of Rydberg states excited to that vibrational level. In practice, these sharp drops in the cross section will be partially masked by structure due to indirect DR,[6,7] which has been ignored in these model calculations. The overall shape of the cross section will, however, follow the shape shown in the figures.

The cross section from v=0 for a potential curve crossing at the large R turning point of v=1 is shown in Fig. 3. As for the case A crossing, the cross section varies as the inverse electron energy at low energies. However, at low electron energies, the cross sections including autoionization for case A are over an order of magnitude larger than those for case B due to the Franck-Condon overlaps. In addition, these smaller overlaps also lead to a lower probability for autoionization so that the solid and dashed curves are nearly coincident. The

breaks above 0.2 eV are once again due to autoionization leaving the ion in excited vibrational levels. The breaks for the v=1 and 2 thresholds are greater than for the case A crossing because of the greater vibrational overlap of the continuum nuclear wave function with these bound vibrational wave functions. At higher energies, the cross section increases with electron energy. This is most easily seen in the dashed curve and is a reflection of the amplitude of the v=0 vibrational wave function. This peaking is the distinctive signature of a large R crossing. At 5 eV, the cross section is about three orders of magnitude larger than the case A cross section. Above 6 eV, the cross section falls off rapidly.

The results for a crossing at the small R turning point of v=1 are shown in Fig. 4. As in the case B crossing, autoionization is unimportant and the two curves are similar at low electron energies. The low-energy cross section is about a factor of ten smaller than that for the case A crossing and about a factor of three larger than the case B cross section. The breaks at higher electron energies can be explained as before. As expected, the cross section for the case C crossing falls off more rapidly with increasing electron energy than for the other two cases.

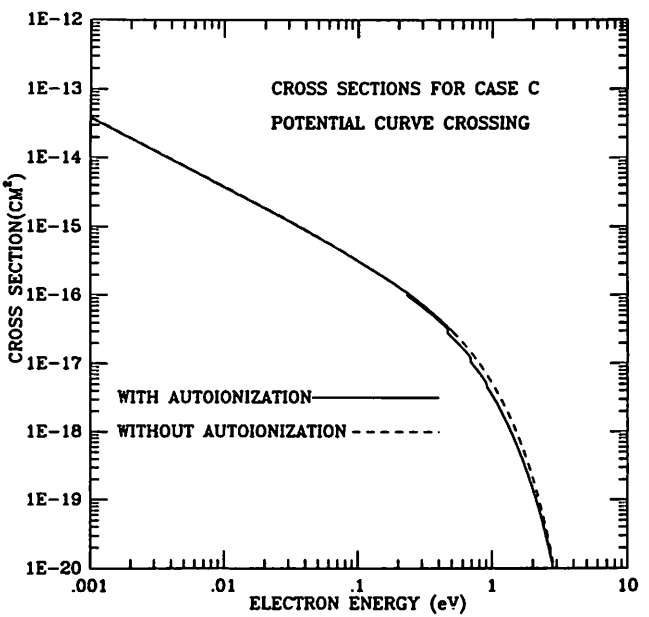

Fig. 4 DR from v=0 for a neutral repulsive potential curve crossing at the small R turning point of the v=1 ion vibrational level.

Assuming a Maxwellian distribution of electron energies, the rate for the recombination α of ion vibrational level v at electron temperature T_e is given by

$$\alpha(T_e,v)=[2^{1.5}/(\pi m)^{0.5}(kT_e)^{1.5}]\int_0^\infty \varepsilon\sigma_v(\varepsilon)e^{-\varepsilon/kT_e}d\varepsilon \qquad (4)$$

where m is the electron mass, k the Boltzmann constant, and ε the electron energy. The rate at a particular ion vibrational temperature is obtained by assuming a Boltzmann distribution of vibrational levels. All cross sections used in the rate calculations include the effect of autoionization, i.e., the second denominator in Eq.(1) is retained. Using the lowest six vibrational levels (see Fig. 1), the rates for the case A crossing are shown in Fig. 5.

For $100<T_e<1000$ K, the rate varies as $T_e^{-0.50}$ for all vibrational temperatures considered here, in agreement with the earlier prediction.[4,9,11] Such a dependence arises from Eq. (4) if σ goes as $1/\varepsilon$ where $\varepsilon=(k_e^2/2m)$. However, at higher temperatures, σ does not vary as $1/\varepsilon$ due to the rapidly changing Franck-Condon overlap. For $1000<T_e<10{,}000$ K and $T_{vib}=300$ K, the rate varies nearly as $T_e^{-0.65}$, while in

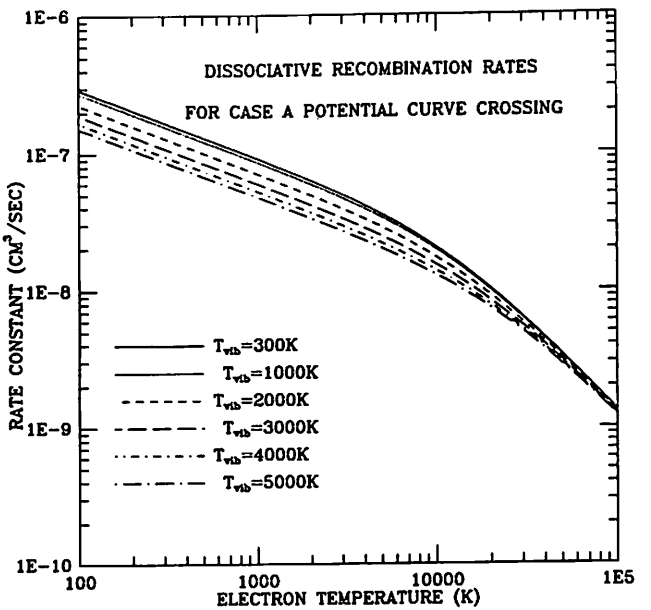

Fig. 5 DR rates for a potential curve crossing near the equilibrium separation of the ion.

the range $10,000<T_e<100,000$ K, the rate varies nearly as $T_e^{-1.2}$. Except at high T_e, the increase in the vibrational temperature T_{vib} from 300 to 5000 K results in a factor of two drop in the DR rate, leading to approximately a $T_{vib}^{-0.25}$ dependence for the rate. For additional discussion of the variation of the rate with T_{vib} and T_e, the reader is referred to Refs. 9 and 10. Note that the rates are nearly independent of T_{vib} at high T_e.

The case B crossing results are shown in Fig. 6. As expected, at low temperatures the rates are about a factor of 20 smaller than the case A rates. Furthermore, the rates now increase with increasing T_{vib} (as $T_{vib}^{+0.63}$ for T_e=300 K and $300<T_{vib}<5000$ K) since the excited vibrational levels have higher Franck-Condon factors than those for v=0. For $100<T_e<1000$ K, the rate varies closely as $T_e^{-0.43}$ for T_{vib}=300 K and as $T_e^{-0.49}$ for T_{vib}=5000 K. For $T_e<5000$ K the case B rates are smaller by about a factor of two than the case A rates for T_{vib}=5000 K. Due to Franck-Condon overlap with the v=0 vibrational wave function, the DR rate increases with T_e for T_{vib}=300 K and for $4000<T_e<20,000$ K. This plateau is the signature of a large R potential curve crossing. Note that the DR rate is approximately independent of vibrational excitation for $T_e>30,000$ K.

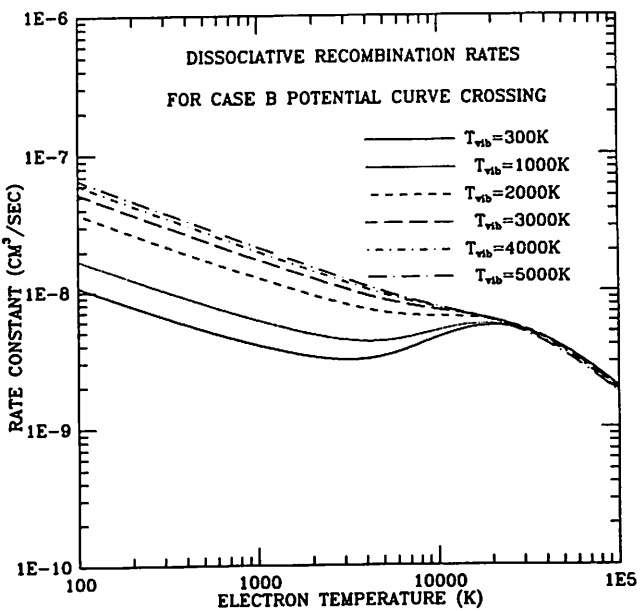

Fig. 6 DR rates for a neutral dissociative potential curve crossing at the large R turning point of the v=1 vibrational level of the ion.

The case C results are shown in Fig. 7. Since the Franck-Condon factors for this curve crossing fall off rapidly with increasing electron energy, these rates are the lowest compared to the other two curve crossings for T_e above 10,000 K. The case C rates increase with increasing T_{vib}. For T_{vib}=5000 K and T_e<1000 K, the rate decreases in nearly the same manner as for case B, i.e., as $T_e^{-0.52}$. However, for T_e>2000 K, compared to case B, there is considerable curvature in the rates. As opposed to the situation for the previous two cases, the rates do not become independent of T_{vib} for high T_e.

The model calculations presented here serve to illustrate the importance of an accurate knowledge of the locations of the intersections of the neutral dissociative routes with the ion potential curve. Additional factors affecting the rates, which have not been considered in these model calculations, are the variation of the widths with internuclear distance and electron energy, indirect recombination, and the superposition of several dissociative routes. The next sections contain a brief description of the application of ab initio theoretical techniques to the determination of potential curves and widths for the

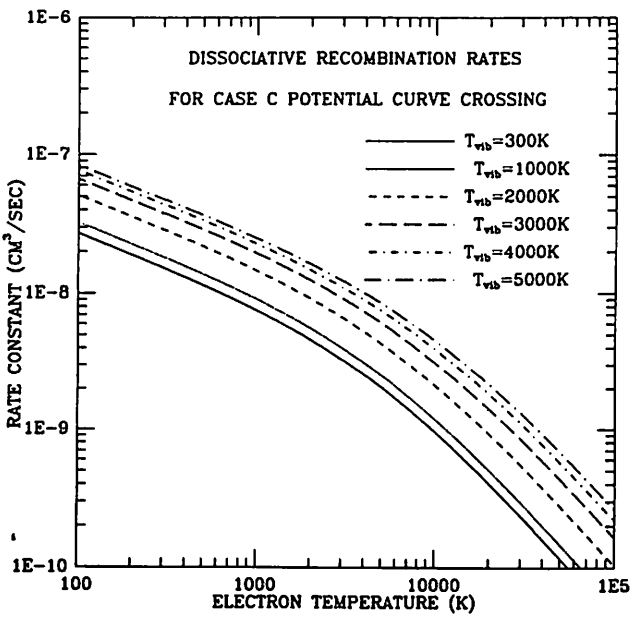

Fig. 7 DR rates for a neutral dissociative potential curve crossing at the small R turning point of the v=1 vibrational level of the ion.

calculation of DR cross sections and rates with results for one particular channel in O_2.

IV. Potential Curves

Contrary to the situation regarding the calculation of electron capture widths (see sec. V), there is a vast literature describing the calculation of molecular electronic potential energy curves. The reader is referred to the volume by Schaefer[11] for a review of several approaches to this problem. A discussion focusing on the calculation of potential curves for the DR of O_2^+, H_2^+, and He_2^+ has already appeared.[12] The reader is referred to Ref. 12 for a review of the approach used here for the calculation of potential curves for O_2^+ and in particular for the dissociative $^1\Sigma_u^+$ route discussed in sec. VI.

In summary, the approach involves the expansion of the molecular orbitals of O_2 in a Gaussian basis set. The coefficients in front of each basis function are determined by multiconfiguration self-consistent field (MCSCF) calculations containing all of the configurations that describe the correct dissociation of the ground state of O_2.[13] For each excited state of a particular symmetry, a reference set of valence configurations is formed by exciting all of the electrons in the valence space, except for the 1σ and 2σ orbitals. From this reference set, all single and double excitations to the virtual orbitals (excluding excitation from the 1σ core orbitals) in which at most a single electron is allowed to occupy the virtual space are included in the configuration interaction (CI) wave function. Such a wave function is referred to as first order[14] CI (FOCI). In the calculations described here, these wave functions have about 2500 terms. Calculations on several O_2 excited states indicate that this approach gives adiabatic excitation energies and dissociation energies that differ from experimentally derived values by about 0.15 eV. Calculated fundamental frequencies differ on average by about 50 cm^{-1} from experiment and equilibrium separations are about 0.06 Bohr larger than experiment.[15,16] Results for all important DR states that dissociate to the valence states of the atoms have been determined.[16]

Figure 8 shows the calculated potential curves that provide dissociative routes leading to the ^1S excited state of atomic oxygen. In the figure, the potential curves for the ground and first excited ion states have been taken from Krupenie.[8] The ion curves have been shifted to larger R to compensate for the difference between the calculated and experimentally derived equilibrium separations of the

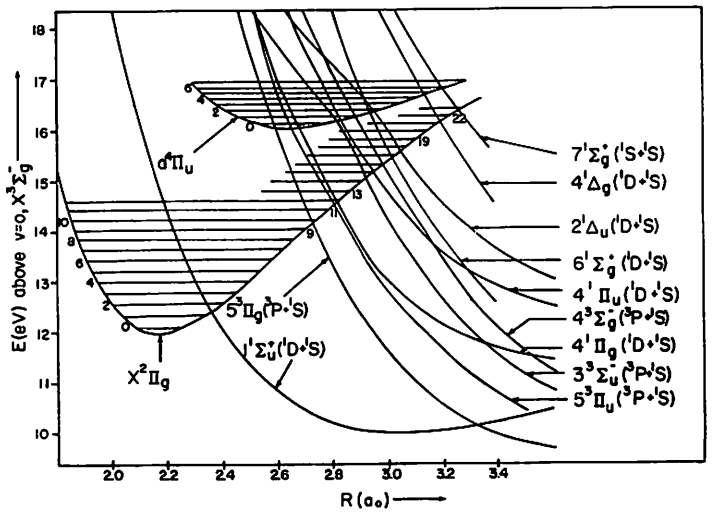

Fig. 8 Calculated potential curves of O_2 providing routes for DR of the ground and lowest metastable states of O_2^+ leading to excited ^1S oxygen atoms.

neutral bound states. The ion curves are also plotted at the experimental excitation energy above the calculated ground state. Shown in parentheses next to the state symbols are the states of the separated atoms that are generated by dissociation along the designated curve. The $^1\Sigma_u^+$ state is the only one that can generate ^1S atoms from the lower vibrational levels of the ground state of the ion. The rate for DR along this route is of great importance to many atmospheric models for which the DR of O_2^+ is a source of the atomic oxygen green line. The next accessible state, $5^3\Pi_g$, crosses the large R turning point of the v=10 level, but can also lead to DR of the v=0 level of the $a^4\Pi_u$ state. The DR of the $a^4\Pi_u$ state along the routes shown in the Fig. 8 can lead to hot atoms with more than 3 eV of translational energy. The $5^3\Pi_u$ state can also lead to the DR of the v=0 level of the metastable ion. However, the $4^1\Pi_g$ state will have a slow rate due to spin considerations.

V. Electronic Widths

There has been very little work reported on the calculation of molecular electronic widths, although there has been some recent important progress.[17] The method outlined below has been used by the author to calculate widths for NO and O_2. Further details will be reported separately.[18] The expression given in Eq. (3) is based on

Fermi's Golden Rule and can be rewritten as

$$\Gamma = 2\pi|\langle P\Psi|H|Q\Psi\rangle|^2 \tag{5}$$

where Ψ is a multiconfiguration wave function and P and Q the Feshbach projection operators[19] that project onto the terms in Ψ representing, respectively, the molecular ion plus a free electron and the autoionizing state. In the usual Feshbach projection operator formalism, an eigenvalue equation is derived for $P\Psi$ that is difficult to solve because it contains an energy-dependent optical potential. However, a new technique[18] based on earlier advances[17,20-22] has been developed in which $P\Psi$ can easily be determined by solving the usual CI problem. Writing the total wave function as $\Psi = P\Psi + Q\Psi$, we can write the Schroedinger equation in matrix form as[20-22]

$$\begin{pmatrix} H_{PP} & H_{PQ} \\ H_{QP} & H_{QQ} \end{pmatrix} \begin{pmatrix} P\Psi \\ Q\Psi \end{pmatrix} \quad E \Gamma \begin{pmatrix} P\Psi \\ Q\Psi \end{pmatrix} \tag{6}$$

where $H_{PP} = PHP$, $H_{QP} = QHP$, etc.

Multiplying the matrices in Eq.(6) leads to:

$$H_{PP}P\Psi + H_{PQ}Q\Psi = EP\Psi \tag{7}$$

and

$$H_{QP}P\Psi + H_{QQ}Q\Psi = EQ\Psi \tag{8}$$

From Eq.(8) we have,

$$Q\Psi = H_{QP}P\Psi/(E - H_{QQ}) \tag{9}$$

Substituting Eq.(9) into Eq.(7) leads to a matrix optical potential for $P\Psi$,

$$(H_{PP} + H_{PQ}H_{QP}/(E - H_{QQ}))\ P\Psi = EP\Psi \tag{10}$$

Since E is on both sides of Eq.(10), it is difficult to solve directly for $P\Psi$. However $P\Psi$ can be easily determined by simply diagonalizing the full H matrix in Eq.(6) and retaining only the coefficients of the $P\Psi$ configurations. In order to divide by $(E - H_{QQ})$ in Eq.(9) and to be certain that $Q\Psi$ does not mix into the $P\Psi$ that is determined by diagonalizing the H matrix in Eq.(6), it is necessary to first solve for the $Q\Psi$ roots by diagonalizing H_{QQ}. The low energy $Q\Psi$ roots are then projected out of the H_{QQ} portion of the H matrix in Eq.(6). $P\Psi$ is then determined by diagonalizing the transformed H matrix. The free electron is represented by a Rydberg orbital with a high principal

quantum number. Successive $P\Psi$ are determined for a series of increasing principal quantum numbers.[18] The widths obtained by this procedure are then extrapolated to the continuum to yield the free electron capture width.

These techniques have been tested on the NO molecule where there are experimentally derived[23] interaction matrix elements for the B and L $^2\Pi$ repulsive states of NO. These states are known[24] to play an important role in the DR of the ground state of NO^+. Using the approach outlined above with a double zeta plus polarization Gaussian basis set and a valence CI for calculation of the entrance and exit channel wave functions, comparison can be made to the experimental results. The experimentally derived width matrix elements have been reported[23] for the lowest NO $^2\Pi$ Rydberg states. Even though the procedure outlined above uses the high (n=7,8) Rydberg states for extrapolation to the continuum width, it is nevertheless instructive to compare our calculated matrix elements for the lowest Rydberg states to the experimentally derived results. For the $B^2\Pi$ repulsive state Hamiltonian matrix element with the $3p\pi$ $C^2\Pi$ Rydberg state, the calculated and experimental[23] results are 1229 and 1382.6 cm^{-1}, while for the $4p\pi$ $K^2\Pi$ Rydberg state the results are 714.2 and 803.9 cm^{-1}, respectively, and for the $5p\pi$ $Q^2\Pi$ Rydberg state the results are 484.8 and 594.6 cm^{-1}, respectively. The difference of only about 11% between theory and experiment for the lower two levels is quite encouraging, considering that the matrix elements are quite small and only small valence space CI wave functions have been used.

Gallusser and Dressler[23] point out that the Q state matrix element is not as reliable as that for the C state, which has the largest matrix element. The experimental Q state matrix element deviates by about 15% from the value predicted from an $n^{*3/2}$ dependence. For the $L^2\Pi$ repulsive state, the calculated and experimental matrix elements with the C state are 546.7 and 549.0 cm^{-1}, respectively, while for the K state the results are 320 and -250 ± 50 cm^{-1}, respectively, and for the Q state we have 218.2 and 200 cm^{-1}, respectively. Gallusser and Dressler[23] have indicated that the Q and K state results are not as reliable as the C state matrix element with which we obtain excellent agreement.

VI. Application to O_2

Using the above procedure for calculation of the width matrix elements combined with the $^1\Sigma_u^+$ potential curve discussed in the previous section, cross sections and rate constants have been determined [using Eqs. (1) and (4)] for

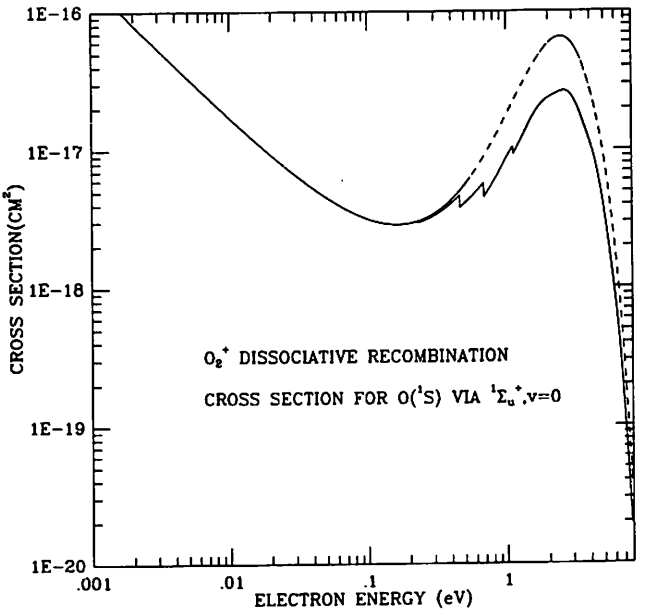

Fig. 9 Cross section for DR from the v=0 level of the ion leading to a ^1S and ^1D O atom.

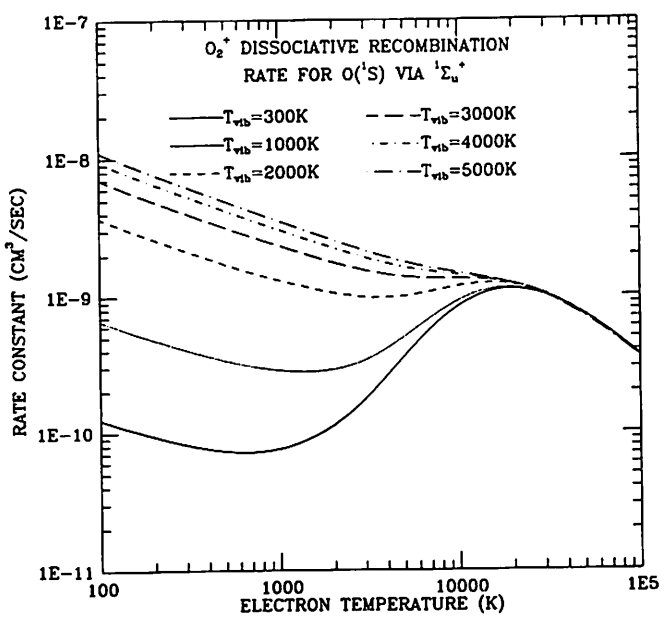

Fig. 10 DR rate along the $^1\Sigma_u^+$ state of O_2 for six vibrational temperatures.

the DR of O_2^+ leading to $O(^1S)$. The ion vibrational wave functions have been approximated with harmonic oscillator functions and the lowest six vibrational levels of the ion have been included. The calculations include the effect of autoionization, i.e., ejection of the electron after capture and before dissociation occurs. The calculations do not include the effect of indirect recombination through intermediate Rydberg states. Figure 9 shows the cross section for DR via the $^1\Sigma_u^+$ state. The shape is characteristic of a case B crossing. However, the slope of the $^1\Sigma_u^+$ curve is only 8 eV/a_o near the ion, compared to the slope of 20 eV/a_o for the model curves. Compared to the 0.30 eV model width, the width calculated here is 0.26 eV from a valence CI wave function having no excitation of the 2σ orbitals. Also, the $^1\Sigma_u^+$ curve crosses the ion above v=1. A further reduction in the cross section is due to the statistical factor r, which is 1.5 in the model calculations, but only 0.25 for the $^1\Sigma_u^+$ cross section.

Figure 10 shows the calculated rates as a function of vibrational temperature. As expected, the rates are sensitive to vibrational temperature at low electron energies, but insensitive at high electron energies where the exponential in the integrand for the rate [see Eq.(4)] allows a wide range of cross sections to be important in the rate integral.

Second-order CI wave functions for O_2 are currently being determined and the rates resulting from these calculations will be reported shortly.[16] Calculations on the other dissociative routes of O_2 and on routes for N_2 and NO are currently in progress. The results will provide DR rate constants, cross sections, atomic quantum yields and translational energies over a wide range of temperatures. The corresponding rate constants and cross sections are difficult to determine experimentally, providing an important opportunity for theoretical contributions to the AOTV modeling effort.

Acknowledgments

The author gratefully acknowledges support of this research at ISR by NASA Ames cooperative agreement NCC 2-308 and at CFA by AFOSR grant 84-0109 and NSF grant ATM-8312742.

References

[1]Park, C., "Radiation Enhancement by Nonequilibrium in Earth's Atmosphere," AIAA Paper 83-0410, Jan., 1983.

[2]Park, C., "Calculation of Nonequilibrium Radiation in AOTV Flight Regimes," AIAA Paper 84-0306, Jan., 1984.

[3]Bates, D. R., "Dissociative Recombination," Physical Review, Vol. 78, 1950, p.492.

[4]Bardsley, J. N., "Configuration Interaction in the Continuum States of Molecules," Journal of Physics B: Atomic and Molecular Physics, Vol. 1, 1968, p.349.

[5]Bardsley, J. N., "The Theory of Dissociative Recombination," Journal of Physics B: Atomic and Molecular Physics, Vol. 1, 1968, p.365.

[6]Giusti, A., Bardsley, J. N., and Derkits, C., "Dissociative Recombination in Low Energy e-H_2^+ Collisions," Physical Review, Vol. A28, 1983, p.682.

[7]Giusti, A., "A Multichannel Quantum Defect Theory Approach to Dissociative Recombination," Journal of Physics B: Atomic and Molecular Physics, Vol. 13, 1980, p.3867.

[8]Krupenie, P. H., "The Spectrum of Molecular Oxygen," Journal of Physical and Chemical Reference Data, Vol. 1, 1972, p.423.

[9]Bardsley, J. N. and Biondi, M. A., "Dissociative Recombination,"Advances in Atomic and Molecular Physics, Vol. 6, 1970, p.1.

[10]Bardsley, J. N., "Temperature Dependence of Dissociative Recombination," Physical Review A:General Physics, Vol. 2, 1970, p.1359.

[11]Schaefer, H. F. III (ed.), Modern Theoretical Chemistry: Methods of Electronic Structure Theory, Plenum Press, New York, 1977.

[12]Guberman, S. L., "Potential Energy Curves for Dissociative Recombination," Physics of Ion-Ion and Electron-Ion Collisions, edited by F. Brouillard and J. W. McGowan, Plenum Press, New York, 1983, p.167.

[13]Guberman, S. L., "Accurate Ab Initio Potential Curve for the Ground State of O_2," Journal of Chemical Physics, Vol. 67, 1977, p.1125.

[14]Schaefer, H. F. III, Klemm, R. A., and Harris, F. E., "First Order Wavefunctions, Orbital Correlation Energies, and Electron Affinities of First-Row Atoms," Journal of Chemical Physics, Vol. 51, 1969, p.4643.

[15]Guberman, S. L., "Potential Curves for Dissociative Recombination of O_2^+," International Journal of Quantum Chemistry, Symposium, Vol. 13, 1979, p.531.

[16]Guberman, S. L., "Dissociative Recombination of O_2^+ with an Electron," in preparation.

[17]Hazi, A. U., "Molecular Resonance Phenomena," Electron-Atom and Electron-Molecule Collisions, edited by J. Hinze, Plenum Press, New York, 1983, p.103.

[18]Guberman, S. L., "An Approach for Calculating Molecular Resonance Widths," in preparation.

[19]Feshbach, H., "Unified Theory of Nuclear Reactions," Annals of Physics (New York), Vol. 5, 1958, p.357.

[20]Lowdin, P. O., "The Calculation of Upper and Lower Bounds of Energy Eigenvalues in Perturbation Theory by Means of Partitioning Techniques," Perturbation Theory and its Application in Quantum Mechanics, edited by C. H. Wilcox, John Wiley and Sons, New York, 1966, p.255.

[21]Lowdin, P. O., "Correlation Problem in Many-Electron Quantum Mechanics, I. Review of Different Approaches and Discussion of Some Current Ideas," Advances in Chemical Physics, Vol. 2, 1959, p.207.

[22]Lowdin, P. O., "Studies in Perturbation Theory. V. Solution of Eigenvalue Problems by Projection Operator Formalism," Journal of Mathematical Physics, Vol. 3, 1962, p.969.

[23]Galluser, R. and Dressler, K. "Multistate Vibronic Coupling Between the Excited $^2\Pi$ States of the NO Molecule," Journal of Chemical Physics, Vol. 76, 1982, p.4311.

[24]Bardsley, J. N., "Dissociative Recombination of Electrons with NO^+ Ions," Planetary and Space Science, Vol. 31, 1983, p.667.